Biointerface Research in Applied Chemistry
Open-Access Journal (ISSN: 2069-5837)

*Article*
**Volume 13, Issue 6, 2023, 580**
https://doi.org/10.33263/BRIAC136.580

# Comparative Study on the Microstructure and Biodegradation Mechanisms of Commercialized Pure Mg and Mg-1.0Ca-0.5Sr Alloy: The Influence of the pH Regulation Techniques

**Nurul Shafyra Binti Mohd Sabri [1], Engku Mohammad Nazim Bin Engku Abu Bakar [1,*], Nor Hasrul Akhmal Bin Ngadiman [1,2], Izman Bin Sudin [1]**

[1] Faculty of Engineering, School of Mechanical Engineering, Universiti Teknologi Malaysia, Johor Bahru 81310, Johor, Malaysia; nurulshafyra@gmail.com (S.S.); nazim@utm.my (E.M.N.); izman@utm.my (S.I.);
[2] Department of Engineering, Faculty of Advanced Technology and Multidiscipline, Universitas Airlangga, Surabaya 60115, Indonesia
* Correspondence: nazim@utm.my (E.M.N.);

Scopus Author ID 36703219700
**Received: 4.11.2022; Accepted: 5.01.2023; Published: 29.03.2023**

**Abstract:** The immersion test in simulated body fluid (SBF) is the most commonly utilized *in vitro* test to reflect an implant's corrosion behavior. Ironically, the influences of the alloying elements on the corrosion behavior were usually concealed by the protective corrosion deposits formed by the specific inorganic species in the SBF. In this study, the effects of the alloying elements on the corrosion behavior of commercially pure magnesium (CP Mg) and Mg-1.0Ca-0.5Sr alloy were determined using 0.9 wt.% NaCl as the corrosion media due to its minor influence on corrosion precipitation and similar osmolality to blood plasma. Their corrosion profile was analyzed using surface characterization techniques and immersion tests, including; (i) hydrogen evolution test ($H_2$), (ii) pH trend, and (iii) weight loss measurement. With the aim of simulating the pH control of the physiological homeostatic process, a pH-buffered pseudo physiological solution was achieved via two techniques; (i) a 24-hour corrosion media renewal routine and through the use of (ii) TRIS-HCL buffer reagent. It is shown that Mg-1.0Ca-0.5Sr alloy exhibits a superior corrosion resistance in both pH regulating treatments, while the effects of the alloying were evident through the corrosion media renewal routine.

**Keywords:** magnesium alloy; corrosion; biodegradable; orthopedic implant.



## 1. Introduction

Bone fracture is conventionally treated by utilizing permanent implants made from metallic biomaterials such as titanium (Ti), 316L stainless steel (316L SS), and cobalt-chromium-molybdenum (Co-Cr-Mo) based alloys [1-3]. These orthopedic implants have been manifested as mechanically efficacious in treating bone fractures. However, employing these permanent implants is associated with multiple major clinical drawbacks, including peri-implant bone loss due to stress shielding, impaired adjacent tissues caused by the release of metal ions, and unexpected pain or discomfort [4, 5]. All of these concerning drawbacks are often solved with the implant removal procedure [6].

However, the implications of the implant removal procedure are continuously debated among medical professionals and have always been a controversial issue. Driessen *et al*. have

reported the incidence of spontaneous femoral neck fracture (SFNF) associated with stress shielding effects, occurring only within 3 weeks after implant (cephalomedullary nail) removal. They have concluded that; the removed implant should be replaced with a shorter cephalomedullary nail to support the stress-shielded bone in order to prevent secondary fracture [7]. This mitigation proposal shows that the implant removal strategy does not stop bone treatment procedures but adds more surgical steps that worsen the patient's morbidity and multiply the treatment cost.

In order to fend off the never-ending bone treatment via orthopedic implant, the risk of stress shielding effect should first be averted. In order to achieve this, a new implant material should be tailored to match the human bone's modulus. Magnesium (Mg), an existing essential element in the human physiological system, exhibits the closest match in modulus value with human bone and has high specific strength and excellent biocompatibility [8, 9]. However, its rapid degradation rate may result in premature loss of mechanical properties, excessive hydrogen gas accumulation, bone resorption, and severe hemolysis [10, 11]. Fortunately, the degradation behavior of Mg can be significantly altered via alloying technique [8, 12]. Since biocompatibility is the most important requirement for a successful implant, nutrient alloying elements are highly favorable in guaranteeing biosafety by promoting excellent hemocompatibility and cytocompatibility [13]. In this study, calcium (Ca) and strontium (Sr) were selected as the alloying elements. Ca, the major component in bone structure, is responsible for bone mineralization [14]. The deployment of Ca as an alloying element can reduce the hypercalcemia risk since it regulates similarly to Mg [15, 16]. Meanwhile, Sr is responsible for promoting bone construction and preventing bone resorption. Thus, it becomes beneficial in treating osteoporosis [17, 18].

Generally, the biodegradation profile of all novel metals or their alloys is assessed in a variety of corrosion media, ranging from a simple saline solution (0.5-3.5 wt.% NaCl) to more complex pseudo physiological solutions, including so-called simulated body fluid (SBF), Hank's balanced salt solution (HBSS), Ringer's solution, phosphate buffered solution (PBS) and cell culture media [19]. These corrosion media shared the same compositional benchmark in which the organic or inorganic ions, protein, and cells are controlled to a value closer to or similar to human blood plasma. However, different Mg alloys may portray an indistinguishable degradation profile due to the similar corrosion protection layer formed by the synergistic reaction between $Ca^{2+}$, $Mg^{2+}$, $HCO_3^-$, and $HPO_4^{2-}$ in the SBF [8]. For this reason, 0.9 wt.% NaCl was chosen as the corrosion media to compare the alloying effect on the corrosion behavior of pure Mg and Mg-1.0Ca-0.5Sr alloy.

Apart from the critical selection of corrosion media when simulating the *in vivo* response, its pH value largely influences the formation and dissolution of the corrosion by-product [20-22]. The excessive $OH^-$ formation may shift the normal physiological pH (7.35-7.45) to a fluctuating pH [23]. The abrupt pH changes may upset the peri-implant tissue by disrupting the protein and cell structures, thus, deteriorating the normal physiological function [24, 25]. Therefore, it is crucial to include a buffering system in corrosion media to avoid discrepancies in biocorrosion behavior and by-products.

4-(2-hydroxylethyl)-1piperazineethanesulfonic acid (HEPES), Tris (hydroxymethyl) aminomethane buffer (Tris-HCL), $NaHCO_3/CO_2$, and phosphate are frequently used as buffering reagents in corrosion media [8, 19, 26, 27]. $NaHCO_3/CO_2$ buffer is commonly recommended due to its capacity to produce $HCO_3^-$ /$H_2CO_3$ buffer [24]. Moreover, it mimics the buffering mechanism established by respiratory control. Comparable *in vivo* results are

proven in several studies. However, its complex setup has made it less desirable to researchers [24]. HEPES and Tris-HCL, on the other hand, offer a simpler experiment preparation and set-up, which can regulate the pH value from 6.8 to 8.2 and 7.0 to 9.0, respectively [28]. Despite their extensive use, HEPES and Tris-HCL do not readily exist in the human body; thus, their utilization may give a deviated biodegradation profile to *in vivo* response. For this reason, a simpler approach to regulating the pH can be achieved by the daily renewal of the corrosion media (24 h interval replenishment). To date, there is no comparative study of the pH regulating techniques on the biodegradation profile of the pure Mg and Mg-1.0Ca-0.5Sr alloy in 0.9 wt.% NaCl.

This work aims to determine the relevant *in vitro* corrosion media for newly developed Mg-based orthopedic implants by elucidating the effect of inorganic ions composition and concentration in pH-regulated systems. To mimic dynamic *in vivo* pH control, 24 h corrosion media renewal was performed, and Tris/HCL buffer reagent was added to the corrosion media. Degradation kinetics and mechanisms were studied by immersion testing, which includes $H_2$ evolution test, pH variation assessment, and mass loss measurement. The corrosion precipitation types and their order of formation with respect to pH value are predicted via Hydra-Medusa simulation and verified by experimental characterization of the corrosion surface and its components.

## 2. Materials and Methods

### *2.1. Sample preparation.*

CP Mg and ternary Mg-Ca-Sr alloy with a nominal composition of 1 wt.% Ca and 0.5 wt.% Sr was prepared using commercially pure Mg ingot (≥ 99%, Sigma Aldrich, St. Louis, MO), Ca granules (99%, Sigma Aldrich, St. Louis, MO), Sr granules (99%, Sigma Aldrich, St. Louis, MO). Prior to the casting process, the CP Mg ingot was carefully cleaned to impede impurities contamination in the alloy system. The CP Mg ingot was cut into small pieces to fit the high-purity graphite crucible. Any oxide layer that readily formed on the Mg ingots' surface was removed by using silicon carbide (SiC) emery paper before being ultrasonically cleaned in acetone for 10 minutes. Following this procedure, the starting materials were melted together in an induction furnace under the protection of a high-purity argon (Ar) atmosphere at 720 °C. A refractory clay mixture was placed around the crucible opening to seal the casting system from possible oxygen contamination. Each melt was held for approximately 45 minutes; the initial 30 minutes were to ensure complete melting of the alloy, and the final 15 minutes were held to allow the melt to form a homogeneous solution. Then, the melted alloy was poured into a preheated mild steel mold (250 °C). Both melt and mold were allowed to be air-cooled. 10mm × 10 mm × 4mm thin plates were sectioned for microstructural analysis, and a disc-shaped sample of ⌀15 mm × 2 mm was prepared for immersion test. All the samples were ground with SiC emery papers up to 2000 grit, polished, and ultrasonically rinsed in acetone for 10 minutes before air drying. The subsequent sample handling was maintained under sterile conditions.

### *2.2. Microstructure characterization.*

The polished and cleaned CP Mg and its alloy were chemically etched with a 2 % nitric acid solution. The microstructure profile variation between CP Mg and Mg-1.0Ca-0.5Sr alloy was examined via an optical microscope (OM) and scanning electron microscope (SEM)

equipped with energy dispersive spectrometry (EDS). At the same time, the surface phase composition was identified by the X-Ray diffraction (XRD) technique.

*2.3. Immersion test.*

Immersion tests were carried out in 0.9 wt.% NaCl in accordance with ASTM-G31-72 at starting pH of 7.4. The temperature of 37 ± 0.5 °C was kept constant using a water bath for 14 days (336 hours). Both solutions were pH controlled via two different routes; (i) 24h corrosion media renewal and (ii) addition of Tris/HCl buffer reagent. To facilitate comparison of the results, the abbreviations for CP Mg and Mg-1.0Ca-0.5Sr alloy in each condition are listed in Table 1.

**Table 1.** Designated abbreviations for CP Mg and Mg-1.0Ca-0.5Sr alloy in three different pH regulating treatments in 0.9 wt.% NaCl.

| | Abbreviation | | |
|---|---|---|---|
| **Condition** | **Uninterrupted (non-renewed)** | **24h corrosion media renewal** | **Tris-HCL buffered** |
| **Material** | 0.9 wt.% NaCl | 0.9 wt.% NaCl | 0.9 wt.% NaCl |
| CP Mg | MgNx | MgNR | MgNT |
| Mg-1.0Ca-0.5Sr | M2Nx | M2NR | M2NT |

The concentrations of the corrosion media components compared to the human plasma are summarized in Table 2. The corrosion media volume to sample surface area (S/A) ratio was set at 1 $cm^2$/40 ml. Due to the rapid pH increase during the early immersion, 1h interval observation on pH and hydrogen release was done for the first 24 hours, while 24 h interval observation was done for the subsequent immersion days. The pH reading was measured via a pH meter (Sartorius, PB-10), while the hydrogen evolution was collected by following the well-established technique [29]. After the designated immersion time, the samples were removed from the corrosion media, carefully rinsed with distilled water, and air-dried. Their surface morphology and corrosion product composition were analyzed via XRD, SEM, and EDS. The mass loss of the samples was calculated after the removal of the corrosion product via chromic acid and silver nitrate solution. Then, the *in vitro* corrosion rate in terms of mass loss and hydrogen evolution was calculated according to the following equation:

$$CR = \Delta m / At \quad (1)$$

where CR is the corrosion rate, mg/$cm^2$/h, Δm is the weight loss, mg (for hydrogen evolution test, 1ml evolved $H_2$ gas = 1.083 mg of Mg), A is the sample initial surface area, $cm^2$, and t is the immersion time, hour. This corrosion rate was the average value of the triplicated immersion test.

**Table 2**. Concentrations of the corrosion media components as compared to the human plasma.

| **Ionic species** | **Ionic concentration (mM)** | | |
|---|---|---|---|
| | **Human Plasma** | **0.9 wt.% NaCl** | **0.9 wt.% NaCl + Tris/HCl** |
| $Na^+$ | 142 | 154 | 154 |
| $K^+$ | 5.0 | - | - |
| $Mg^{2+}$ | 1.5 | - | - |
| $Ca^{2+}$ | 2.5 | - | - |
| $Cl^-$ | 103 | 154 | 154 |
| $HCO_3^-$ | 27.0 | - | - |
| $HPO_4^{2-}$ | 1.0 | - | - |
| $SO_4^{2-}$ | 0.5 | - | - |
| Tris | - | - | 50.5 |

*2.4. Corrosion precipitation prediction via Hydra-Medusa.*

The possible formation of corrosion by-products related to pH value was simulated by Hydra-Medusa software. All ionic components in respected corrosion media were specified in Hydra software. The concentration of these components was then specified in Medusa software to predict the possible formation of corrosion deposits at different pH values. However, the concentration of $Mg^{2+}$, $Ca^{2+}$, and $Sr^{2+}$ was obtained by adding the final ionic concentrations (calculated from the evolved $H_2$) to their initial concentration. The simulated diagram of precipitation fraction vs. pH value with respect to $Mg^{2+}$ and $Ca^{2+}$ was merged into a single diagram to present the final potential precipitations.

## 3. Results and Discussion

*3.1. Cp Mg and Mg alloy microstructure and phase constitution characterization.*

The as-cast CP Mg and Mg-1.0Ca-0.5Sr alloy and its constituents were examined via OM, SEM, EDS, and XRD techniques to elucidate the influence of alloying elements on the Mg's metallographic configuration. Table 3 summarizes the overall chemical composition of the as-cast CP Mg and Mg-1.0Ca-0.5Sr alloy, where a tallied value between the nominal composition and the detected Mg, Ca, and Sr percentages were observed, thus, implying the adequacy of the casting process. A notable difference between CP Mg and Mg-1.0Ca-0.5Sr alloy was depicted in Figure 1, where CP Mg displays a single-phase structure with significantly large grains (510 ± 22 µm). Due to its large grain size, the obtained XRD spectra (Figure 2) were very sharp and perfectly matched the pure Mg peak (JCPDS No. 98-006-221) with no additional precipitates or impurities peak.

**Table 3.** Elemental comparison between the nominal content and EDS analyzed value**.**

| Mg system | Mg (wt.%) | | Ca (wt.%) | | Sr (wt.%) | |
|---|---|---|---|---|---|---|
| | Nominal | Detected | Nominal | Detected | Nominal | Detected |
| CP Mg | 100.0 | 99.8 | 0 | 0.1 | 0 | 0 |
| Mg-1.0Ca-0.5Sr | 98.5 | 98.3 | 1.0 | 1.2 | 0.5 | 0.5 |

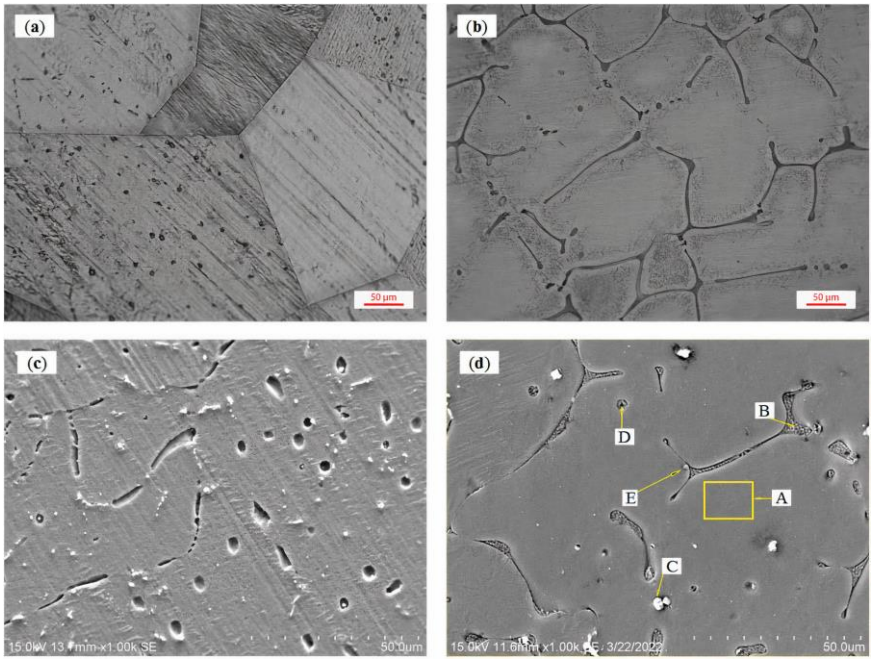


**Figure 1.** Optical microstructure of (**a**) CP Mg; (**b**) Mg-1.0Ca-0.5Sr and their corresponding SEM images; (**c**) CP Mg; (**d**) Mg-1.0Ca-0.5Sr.

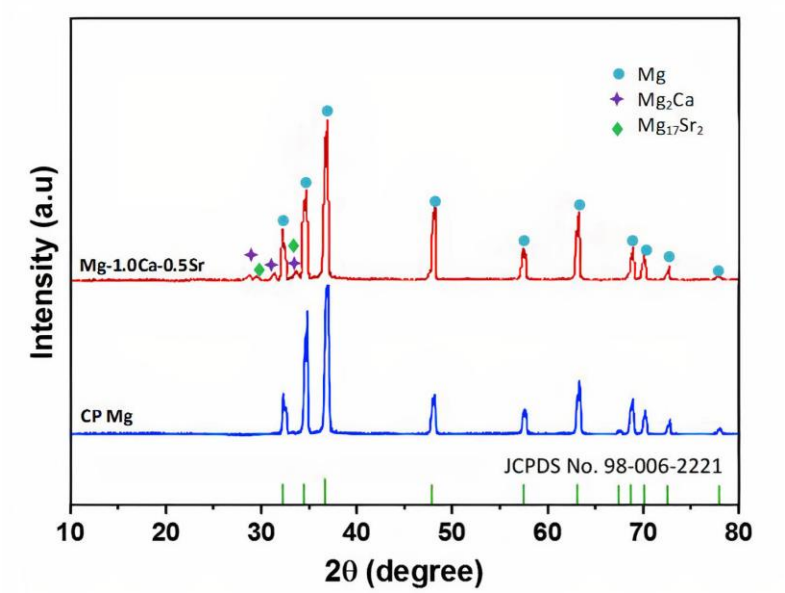


**Figure 2.** The XRD spectra of as-cast CP Mg and Mg-1.0Ca-0.5Sr alloy.

In contrast, Mg-1.0Ca-0.5Sr exhibits irregular ellipsoidal-shaped α-Mg dendrites with saturated intermetallic phases within the lamellar structure in the GBs (Figure 1(b) and (d)). The elemental constituents at multiple sites across the micrograph were analyzed via EDS and listed in Table 4. The α-Mg matrix (area A) in Figure 1(d) was found to contain the highest amount of Mg, while the lamellar structure in the GBs was saturated with Ca and Sr eutectic phases (point B). A random distribution of these intermetallic phases was also traced in the dendritic region, where the amount of Sr-rich Mg dominates. It appears as a bright globular particle (point C), while the greyish globular phase (point E) contains only Mg and Ca elements. According to the thermodynamic phase diagram of the ternary Mg-Ca-Sr system, the phases in the area or spot A, B, C, E, are identified as Mg, a mixture of $Mg_2Ca$ and $Mg_{17}Sr_2$, $Mg_{17}Sr_2$ and $Mg_2Ca$ respectively. Figure 2 displays the XRD spectrum of the CP Mg and Mg-1.0Ca-0.5Sr, confirming the presence of the expected $Mg_2Ca$ and $Mg_{17}Sr_2$. These results were in accord with the published reports [30,31].

**Table 4.** Chemical composition analysis of Mg-1.0Ca-0.5Sr by EDS, wt.%.

| Analysis site | Detected element (wt. %) | | |
|---|---|---|---|
| | **Mg** | **Ca** | **Sr** |
| A (α-Mg interior) | 99.5 | ≈0 | ≈0 |
| B (GB interior) | 65.0 | 15.0 | 20.0 |
| C (bright globular particle) | 75.3 | 0 | 24.7 |
| D (globular lamellar) | 65.8 | 9.3 | 24.9 |
| E (greyish globular phase) | 33.7 | 66.3 | 0 |

Morphologically, it is evident that the grain size of Mg-1.0Ca-0.5Sr was significantly refined to 96 ± 10 μm when both Ca and Sr were introduced into the Mg system. This refinement effect was due to the enrichment of the solute undercooling (ΔT), in which its pivotal influence on the as-cast grain size and intermediate phase formation was correlatively described via the growth restriction factor (GRF), *Q* [32]. By utilizing a binary Mg-*A* phase diagram (*A*: alloying element), $Q_{total}$ can be calculated by the following formula:

$$Q_{total} = \sum m_i . C_{0,i} (k_i - 1) \quad (2)$$

where $m_i$ is the gradient of the liquidus line (the curved liquidus line was assumed to be straight), $k_i$ is the solute's equilibrium partition coefficient, and $C_{0,i}$ is the element *i*'s initial concentration [33]. A greater *Q* value indicates a higher ΔT at the growing dendrite front. The

value of $m$, $k$, and $Q$ ($m(k_i - 1)$) for Mg-Ca and Mg-Sr are listed in Table 5. Since the solubility limit of Ca and Sr in α-Mg is relatively low (1.34 wt.% and 0.11 wt.% respectively), Sr and Ca rapidly enriched in the front of the solid/liquid interface as the act of rejecting the alloying elements, thus, inhibiting the grain growth during solidification of the melt. In this study, $Q_{total}$ for Mg-1.0Ca-0.5Sr was highly contributed by $Q_{1.0Ca}$, which the $Q_{total}$ is the sum of $Q_{1.0Ca}$ (11.9098) and $Q_{0.5Sr}$ (1.75441), indicating a dominant grain refinement effect contributed by 1.0 wt.% Ca. This value is in good agreement with the EDS analysis in Figure 1(d), point B, where the β-eutectic phases in the GB contain more Ca than Sr. Similar grain refining effect induced by Ca was reported by previous studies [34-37].

**Table 5.** GRF, Q value for the Mg-Ca and Mg-Sr binary systems[38-39].

| Alloying element | *m* | *k* | *m*(*k* – 1) | System |
|---|---|---|---|---|
| Ca | -12.67 | 0.06 | 11.94 | Mg-Ca eutectic |
| Sr | -3.53 | 0.006 | 3.51 | Mg-Sr eutectic |

*3.2. Post-immersion: Morphology analysis and corrosion precipitation characterization.*

Figure 3 displays the corrosion morphologies of CP Mg and Mg-1.0Ca-0.5Sr in 0.9 wt.% NaCl. There are three treatment groups in each corrosion media ; (i) without corrosion media renewal (controlled system), (ii) with 24h corrosion media renewal, and (iii) with Tris-HCL buffer reagent addition. The effects of CP Mg and Mg-1.0Ca-0.5Sr alloy under these pH regulation techniques on the corrosion profile were qualitatively and quantitatively compared.

During the 14 days immersion period in 0.9 wt.% NaCl, all CP Mg in the three treatment variants (Figure 3(a-c)) were covered with a white cauliflower-like precipitate. However, each of them has experienced a different degree of degradation, where the MgNx shows a uniform corrosion deposit across the surface. Meanwhile, a small cavity (70.085 µm) and deepened grooves were observed on MgNR.

In Tris-HCL buffered 0.9 wt.% NaCl, MgNT displays much-severed corrosion protection breakdown where a larger void (271.784 µm) has been formed, exposing the CP Mg substrate. The appearance of the greyish-flat surface indicates the least affected region, known as the cathodic region. Its level distribution over the surface area indicates a uniform spread of precipitation coverage throughout the immersion period. EDS analysis in Table 6 has shown that the elements of the corrosion deposit are Mg, O, Cl, and C, indicating the presence of $Mg(OH)_2$ and a trace of $MgCl_2$.

**Table 6.** Elemental composition of CP Mg and Mg-1.0Ca-0.5Sr alloy corrosion product via EDS analysis. Spots and area analysis (A-L) are indicated in Figure 3.

| Material | Treatment condition | Analysis site | Elements (at.%) | | | | | |
|---|---|---|---|---|---|---|---|---|
| | | | Mg | O | C | Cl | Ca | Sr |
| CP Mg | Non-renewed | A | 4.3 | 79.4 | 15.5 | 0.8 | - | - |
| | | B | 70.4 | 23.4 | 6.0 | 0.2 | - | - |
| | 24h renewal | C | 3.2 | 72.9 | 22.3 | 1.6 | - | - |
| | | D | 24.65 | 60.45 | 3.5 | 11.4 | - | - |
| | Tris-HCL buffered | E | 2.8 | 76.5 | 19.5 | 1.2 | - | - |
| | | F | 45.8 | 43.7 | 10.2 | 0.3 | - | - |
| Mg-1.0Ca-05Sr | Non-renewed | G | 5.4 | 75.8 | 18.3 | - | 0.1 | 0.4 |
| | | H | 78.1 | 17.8 | 3.1 | - | 0.6 | 0.4 |
| | 24h renewal | I | 80.8 | 12.2 | 6.7 | - | 0.3 | - |
| | | J | 27.5 | 59.4 | 11.2 | 1.2 | 0.3 | 0.4 |
| | Tris-HCL buffered | K | 89.7 | 7.8 | 1.7 | - | 0.8 | - |
| | | L | 25.1 | 66.9 | 6.5 | 1.5 | 0 | - |

It is noticeable that the Cl content is higher for MgNR, indicating a higher level of corrosion rate induced by the 0.9 wt.% NaCl renewal routine. However, $MgCl_2$ remains undetected in XRD analysis, which may be due to its leaching during the sample cleaning procedure [40, 41].

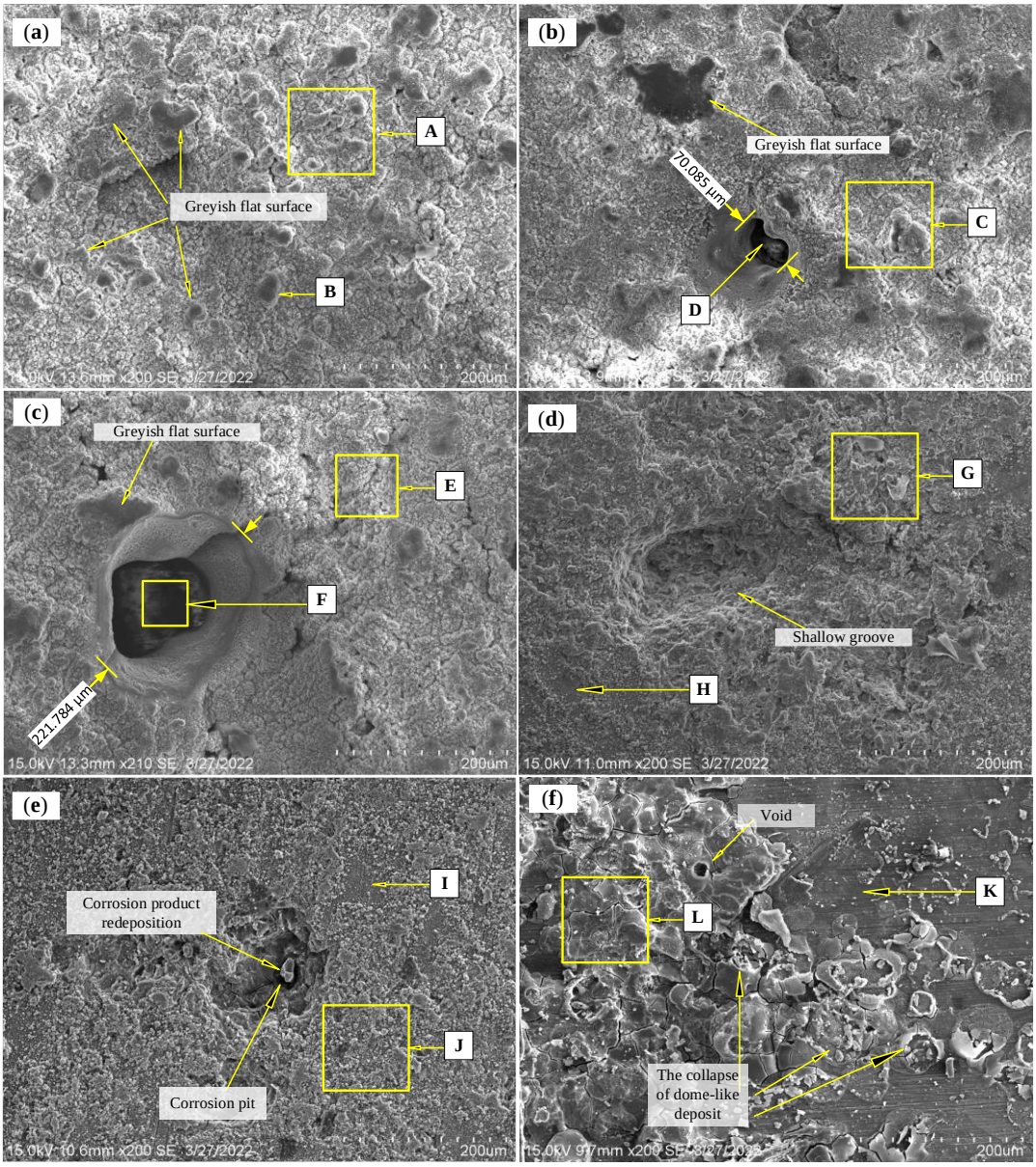


**Figure 3.** SEM image of the degraded surface of CP Mg and Mg-1.0Ca-0.5Sr alloy in 0.9 wt.% NaCl corrosion media post 14 days immersion: (**a**) MgNx; CP Mg in uninterrupted saline solution (without corrosion media renewal); (**b**) MgNR; CP Mg in interrupted saline solution (with corrosion media renewal); (**c**) MgNT; CP Mg in Tris-HCL buffered saline solution; (**d**) M2Nx; Mg-1.0Ca-0.5Sr alloy in uninterrupted saline solution (without corrosion media renewal); (**e**) M2NR; Mg-1.0Ca-0.5Sr alloy in interrupted saline solution (with corrosion media renewal); (**f**) M2NT; Mg-1.0Ca-0.5Sr alloy in Tris-HCL buffered saline solution. (EDS compositional spot and area analysis obtained from different labeled points is summarized in Table 6).

However, the degree of degradation was much lower in Mg-1.0Ca-0.5Sr alloy due to forming a more compact corrosion precipitate than porous cauliflower-like deposits, providing greater protection against corrosive media infiltration into its substrate (Figure 3 (d-f)) in the uninterrupted 0.9 wt.% NaCl, a coarse and flaky corrosion scale was formed with a formation of a shallow crater on its surface. However, a grainy corrosion deposit with a much deeper localized pit was seen when the renewal routine of 0.9 wt.% NaCl was employed. Evidence of

continuous dissolution-precipitation kinetics to establish an equilibrium state can be seen in the 0.9 wt.% NaCl replenishment routine through the redeposition of $Mg(OH)_2$ on top of the pit surface (Figure 3(e)). In addition, there are some regions that are still flat and uncovered by the corrosion product, as in point I, indicating a preferential corrosion phenomenon due to micro-galvanic difference. This is verified by EDS analysis where the Mg content is very high (80.8 at.%), indicating an area of delayed degradation or could play a cathodic role.

Understanding the corrosion resistance of a newly designed Mg alloy requires a basic knowledge of the dissolution reaction of pure Mg as a foundation [42, 43]. Mg is generally known for its accelerated degradation in aqueous media that generates $H_2$ gas and precipitates magnesium hydroxide (Equation 3-6) [44,45].

| | | |
|---|---|---|
| $Mg \rightarrow Mg^{2+} + 2e^-$ | (anodic partial reaction) | (3) |
| $2H_2O + 2e^- \rightarrow H_2 + 2OH^-$ | (cathodic partial reaction) | (4) |
| $Mg^+ + 2H_2O \rightarrow Mg^{2+} + 2OH^- + H_2$ | (overall reaction) | (5) |
| $Mg^{2+} + 2OH^- \rightarrow Mg(OH)_2$ | (corrosion product) | (6) |

This simultaneous dissolution-precipitation kinetics in Equations (3) and (6) are demonstrated in the Mg alloy in Figure 3(e-f), where a distinct anodic and cathodic region and corrosion deposit were observed due to the formation of secondary phases. As mentioned, the secondary phases formed in the Mg-1.0Ca-0.5Sr alloy have been verified as $Mg_2Ca$ and $Mg_{17}Sr_2$. Although most studies suggest that $Mg_2Ca$ acts as an anode, there have been several conflicting views on the potential nature of $Mg_2Ca$ in galvanic corrosion. Jung *et al*. have reported that $Mg_2Ca$ exhibits a cathodic property relative to the α-Mg matrix. Whereas Kim *et al*. have declared a negligible potential difference between the α-Mg matrix and $Mg_2Ca$. However, in this study, the anodic nature of $Mg_2Ca$ is displayed where the $Mg_2Ca$ in GBs preferentially corrodes, while the neighboring α-Mg became cathodic protected via the formation of a thin white hydroxide layer next to the anodic GBs. During our experimental immersion test, simultaneous $H^2$ evolution and the preferential accumulation of $OH^-$ bubbles at the cathodic sites on the Mg-1.0Ca-0.5Sr alloy surface were clearly evident in Figure 4.

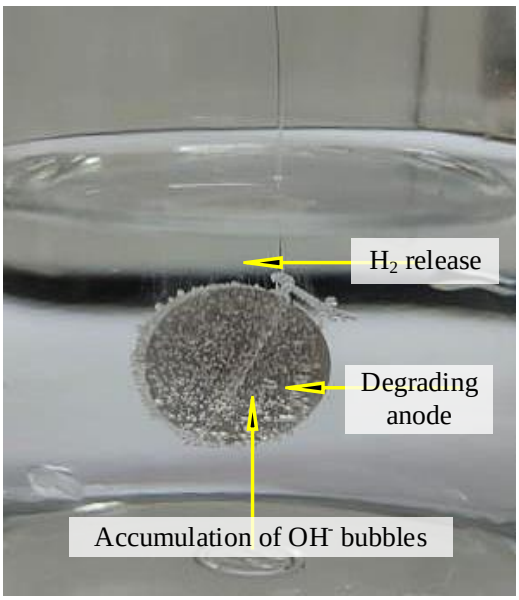


**Figure 4.** Photograph of Mg-1.0Ca-0.5Sr alloy immersed in 0.9 wt.% NaCl corrosion media, showing the effects of micro-galvanic corrosion where a simultaneous accumulation of $OH^-$ bubbles over the higher potential area (cathode) and the rapid $H_2$ evolution due to the dissolving anode.

$Mg_{17}Sr_2$, on the other hand, exists in GBs as well as in the α-Mg matrix. There is also debate on the electro-potential nature of $Mg_{17}Sr_2$. For instance, Thekkepat *et al*. calculated the electrochemical potential of Mg, $Mg_{17}Sr_2$ based on the Born-Haber cycle and reported that $Mg_{17}Sr_2$ serves as an anode due to its lower electrochemical potential ($E_{Mg}$ = -2.37 V and $E_{Mg17Sr2}$ = -2.387 V) [46]. This finding was experimentally supported by Liu *et al*., where $Mg_{17}Sr_2$ has preferentially corroded, releasing $Sr^{2+}$ ions into the corrosion media. However, a nobler nature of $Mg_{17}Sr_2$ over Mg was exhibited by multiple research [46, 47] in which the adjacent α-Mg matrix rapidly dissolved, leaving $Mg_{17}Sr_2$ at the GBs. However, this study agreed with the latter. Since $Mg_2Ca$ is the most anodic phase compared to α-Mg matrix and $Mg_{17}Sr_2$, it was preferentially corroded, leaving $Mg_{17}Sr_2$ as the matrix skeleton. The higher potential of $Mg_{17}Sr_2$ converts the previous cathodic α-Mg matrix into an anodic mode in which the corrosion propagates from the α-Mg matrix area adjacent to $Mg_{17}Sr_2$ to its center. However, the α-Mg matrix surrounded by $Mg_{17}Sr_2$-deficient GBs may detach from the alloy as the $Mg_2Ca$ corrodes intergranular, resulting in shallow craters [48, 49], as shown in Figure 3 (d). However, the region with a high-volume fraction of $Mg_{17}Sr_2$ can protect the Mg matrix from further degradation, where the continuous $Mg_{17}Sr_2$ network acts as a corrosion barrier [47, 50].

Meanwhile, Figure 3 (f) demonstrates a completely different corrosion morphology when the Mg alloy was immersed in Tris-HCL buffered saline. Uneven corrosion precipitation coverage was observed where a thick corrosion agglomeration with multiple cracks (Area L) and the volcano-like crater was present in one area, while the other area was not visibly protected (Area K), indicating an unstable surface activity during the immersion period. In addition, partial dissolution of the corrosion protection layer is evident by the collapse of the thin, rounded dome-like corrosion deposits. As mentioned, the increase of pH value in corrosion media was due to the generation of $OH^-$ from Mg dissolution. Meanwhile, Tris-HCL regulates the corrosion media's pH value by consuming the generated $OH^-$ ions from equation (4) by its bonded $H^+$, hence suppressing the formation of $Mg(OH)_2$ precipitates that require $OH^-$ ions (Equation 6) [22, 51]. This reaction, therefore, suggests that the addition of Tris-HCL in saline solution has severely degraded both CP Mg and Mg-1.0Ca-0.5Sr due to continuous surface activation via $OH^-$ consumption. Ironically, in MgNT, there was no evidence of bare surface, which might contradict the $OH^-$ consumption tendency imposed by the Tris-HCL buffer reagent observed in M2NT. There are three contributing factors that explain this surface profile, which is (i) due to the significantly fast dissolution of CP Mg, excess $OH^-$ ions are accumulated; therefore, despite its consumption by Tris-HCL buffer reagent, this ion is sufficient for $Mg(OH)_2$ precipitation, (ii) the Tris-HCL buffer reagent was completely depleted towards the end of the immersion time, whereas the $OH^-$ ions were continuously produced, allowing $Mg(OH)_2$ to precipitate, and (iii) Tris-HCL buffer reagent regulate pH in the bulk corrosion media, rather than the local pH at CP Mg interface [51].

Although different substrate materials were studied, the XRD analysis in Figure 8 depicts that $Mg(OH)_2$ is the only deposit formed in both CP Mg and Mg-1.0Ca-0.5Sr alloy, thus, revealing that the alloying technique does not contribute to a novel corrosion shield in 0.9 wt.% NaCl corrosion media. It is important to note that $Mg(OH)_2$ only provides semi-protection property due to its higher solubility at lower pH and high susceptibility to the $Cl^-$ attack [52, 53]. However, this insufficient protection by Mg(OH)2 reflects more insight into the substrate itself [19].

However, the degree of corrosion to which metals are exposed should not be determined solely by assessing the amount of precipitation coverage. For instance, a scarcity of passivation

layer coverage may signify poorer corrosion protection as well as indicate delayed degradation or enhanced corrosion resistance. Therefore, the post-immersion surface evaluation must be supported by the $H_2$ evolution test and mass loss measurement.

*3.3 Influence of pH regulation approaches in 0.9 wt.% NaCl.*

Figure 5 (a) shows the plotted evolved $H_2$ volume against immersion time for CP Mg and Mg-1.0Ca-0.5Sr alloy in saline media under three treatment conditions. The $H_2$ evolution test is an excellent yet simple technique for evaluating the *in vitro* corrosion rate of metals in aqueous media. Since the dissolution of Mg is accompanied by pH variation, the $H_2$ evolution test is complemented by the pH trend test (Figure 5 (b)) to reflect each metal's corrosion rate and behavior in different ph regulation treatments. It is generally accepted that the dissolution of Mg generates $OH^-$ ions that shift the system's pH to a higher basic level [54-55]. Meanwhile, Figure 5(c) displays the calculated degradation rate in terms of released $H_2$ volume and mass loss.

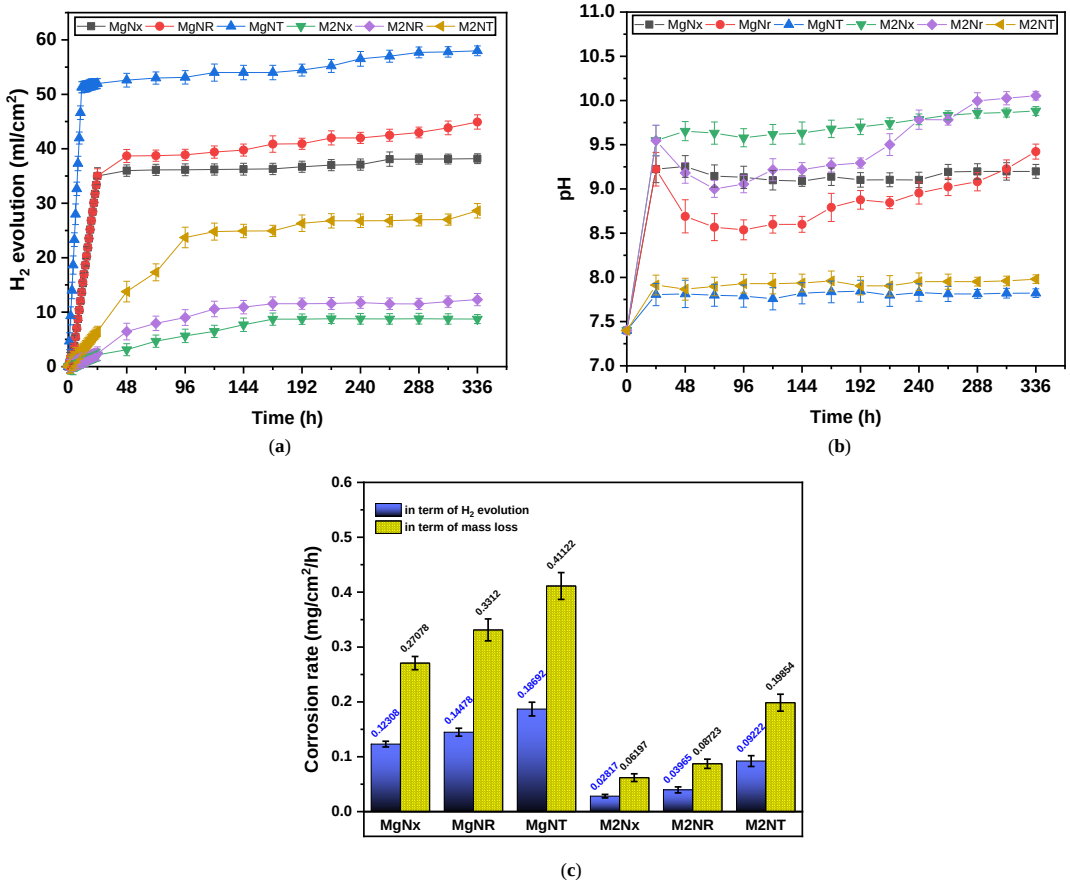


**Figure 5.** Immersion test results of CP Mg and Mg-1.0Ca-0.5Sr alloy in 0.9 wt.% NaCl corrosion media. (**a**) $H_2$ release volume per surface area in different pH regulating treatments, (**b**) time dependant pH variation, and (**c**) corrosion rate in terms of mass loss and evolved $H_2$. The legends in (**a**) and (**b**) indicate the respective materials in corresponding treatment conditions, as summarized in Table 1.

From Figure 5 (a), both CP Mg and Mg-1.0Ca-0.5Sr alloy follow the same evolution trend under all treatment conditions, where abrupt $H_2$ release was observed in the early immersion phase, suggesting rapid dissolution of the anode that is striving for a dynamic equilibrium state [56]. Then, the $H_2$ release slowed down before reaching a stabilized evolution rate. This profile may be attributed to the gradual growth of protective precipitation coverage across the surface.

In the immersion test with 24h saline renewal, the $H_2$ evolution rate for both CP Mg and Mg-1.0Ca-0.5Sr alloy experienced an increased rate after the first corrosion media replacement (at 24h to 48h). It was found that CP Mg experienced a steeper $H_2$ evolution curve under all treatment conditions but leveled off earlier than the Mg-1.0Ca-0.5Sr alloy under all treatment conditions. However, continuous dissolution was observed in both CP Mg and Mg-1.0Ca-0.5Sr alloy in the renewed and buffered saline solution, in which CP Mg and Mg-1.0Ca-0.5Sr alloy demonstrated an up-steady-up-steady-up $H_2$ evolution tendency and a continuously climb until the end of immersion time. The fluctuating and continuous $H_2$ evolution of the Mg-1.0Ca-0.5Sr alloy in buffered saline indicates a difficulty in reaching a maintained equilibrium state, while the continuous $H_2$ evolution in MgNR may be attributed to the lowest potential of CP Mg and the increased $Cl^-$ ions exposure resulting from the 0.9 wt.% NaCl renewal routine.

Among the three treatment conditions, it is apparent that adding Tris-HCL buffering reagents into the saline solution has escalated both CP Mg and Mg-1.0Ca-0.5Sr alloy dissolution rate than in the immersion with or without corrosion media renewal. On the contrary, the immersion test without corrosion media renewal has demonstrated the lowest $H_2$ evolution, signifying the lowest degradation degree experienced by both CP Mg and Mg-1.0Ca-0.5Sr alloy, as depicted in Figure 5 (c).

A widely agreed hypothesis on the relationship between pH value and $H_2$ release states that the high pH value of the corrosion media always denotes better corrosion resistance in saline solution (low $H_2$ release). This is due to the improved protective capacity provided by the compact $Mg(OH)_2$ that forms at higher pH compared to the porous $Mg(OH)_2$ precipitate that is produced at a lower pH level. Therefore, the lowest pH variation demonstrated by CP Mg and its alloy in Tris-HCL buffered saline explains their highest evolution rate in the $H_2$ evolution test. This hypothesis is also confirmed by the Mg-1.0Ca-0.5Sr alloy in all treatment conditions, where the final pH value of this alloy is higher than the corresponding pH value shown by CP Mg. For instance, the final M2NR's pH is higher than that of MgNR, as is the pH value of M2Nx and M2NT to the MgNx and MgNT, respectively.

As mentioned, the increase of pH value in corrosion media was due to the generation of $OH^-$ from Mg dissolution. Meanwhile, Tris-HCL regulates the corrosion media's pH value by consuming the generated $OH^-$ ions (Equation (4)) by its bonded $H^+$, hence suppressing the formation of precipitates that requires $OH^-$ ions. This reaction, thus, explains their deleterious corrosive attack at lower pH [22, 51, 57]. In addition, Tris is known as a strong chelating agent which forms weak complexes with the dissolved cations within the corrosion media, deviating the cations away from the Mg surface, delaying or inhibiting the precipitation of the protective layer [8, 58].

However, MgNR and M2NR exhibit a lower fluctuating pH value before exceeding the pH value of MgNx and MgNR with pH interception at hours 312 and 240, respectively. These pH trends are inconsistent with the mentioned hypothesis, in which their higher pH value does not indicate a lower dissolution rate as compared to MgNx and M2Nx. This hypothesis rejection is due to; (i) the continuous supply of aggressive $Cl^-$ ion within the bulk corrosion media, generating more pH-raising ions (Equation (8)) and (ii) the bulk detachment of $Mg(OH)_2$ due to the abrupt pH dive soon after the corrosion media renewal, exposing the underlying Mg. Figures 3 (b) and (e) clearly show a higher degree of corrosion attack suffered by CP Mg and Mg-1.0Ca-0.5Sr alloy when the 0.9 wt.% NaCl was replaced daily. As mentioned, $Mg(OH)_2$ is the only corrosion precipitation produced in saline solution. From Figure 5 (b), the sudden drop of pH observed at hour 48 was accompanied by a drastic increase

in $H_2$ evolution within the same immersion time. This trend has indicated a correlation between corrosion rate or $H_2$ evolution with the pH variation where the intermittent deterioration of protection coverage happens after each renewal routine. According to equation (7), the solubility equilibrium of $Mg(OH)_2$ was influenced by the pH value [59, 60];

$$\text{Log } [Mg^{2+}] = 16.95 - 2pH \quad (7)$$

For instance, the pH of M2NR dropped from 9.223 to 7.4 during the first corrosion media renewal, which increased the $Mg^{2+}$ solubility to thousands of fold degrees (0.0319 to 144.2538), indicating a significant increase in $Mg(OH)_2$ solubility that leads to the passivation breakdown which exposed back the Mg substrate to the mass corrosion attack. In addition, the daily renewal of 0.9 wt.% NaCl has cause an increase $Cl^-$ attack on $Mg(OH)_2$, transforming the hydroxide layer into a highly soluble $MgCl_2$ as in the following equation [40]:

$$Mg(OH)_2 + 2Cl^- \rightarrow MgCl_2 + 2OH^- \quad (8)$$

However, the pH started to increase despite of corrosion media renewal routine at hour 72 onwards. This is due to the excessive $OH^-$ accumulation from the water reduction reaction as well as the pH-raising reaction from $Mg(OH)_2$ to $MgCl_2$ conversion (Equation 8). The dissolution of $MgCl_2$ into the corrosion media has exposed the underlying Mg substrates to the corrosive species back again. At this rate, the secondary hydroxide precipitation increased to double the volume of the initial hydroxide, which has caused the intermittent constant pH despite the corrosion media renewal routine [59]. Consequently, the increase in $Mg(OH)_2$ thickness led to its dehydration at the $Mg(OH)_2$/Mg interface due to restricted corrosion media absorption, thereby converting the formed $Mg(OH)_2$ to MgO [59, 61, 62];

$$Mg(OH)_2 \rightleftharpoons MgO \pm H_2O \quad (9)$$

This formation of MgO underneath the $Mg(OH)_2$ layer has further blocked the infiltration of corrosive media to the Mg substrate, causing the pH trend to reach a quasi-constant state at a longer immersion time [61]. However, MgNR displays a continuous pH climb until the end of immersion, indicating the combined effect of accelerated corrosion rate by CP Mg and the excessive attack of $Cl^-$ on $Mg(OH)_2$. This is proven by the large black cavity observed, which indicates a mass Mg shedding due to the renewal routine [62, 63]. In addition, the grain refining effect provided by the Ca and Sr has led to a more compact $Mg(OH)_2$ precipitation, improving the corrosion resistance of the protective barrier [31, 56].

Despite the higher dissolution rate caused by the corrosion renewal routine compared to the uninterrupted treatment, the maintained $Cl^-$ concentration in saline solution mimics the physiological homeostasis response in which all ionic concentrations are always kept constant. In Figure 6, MgNR has shown less white corrosion sediment at the bottom of the test tube. In contrast, immersion tests without corrosion media renewal and with Tris-HCl addition have shown a higher amount of unregulated corrosion sediment that settled at the bottom of the test tube. This phenomenon does not reflect the physiological response to extraneous precipitation, in which the corrosion products are regulated by both macrophage uptake and urinary excretion [64]. Moreover, $MgCl_2$, the product from Equation 8, was reported to be more corrosive than NaCl itself [65].

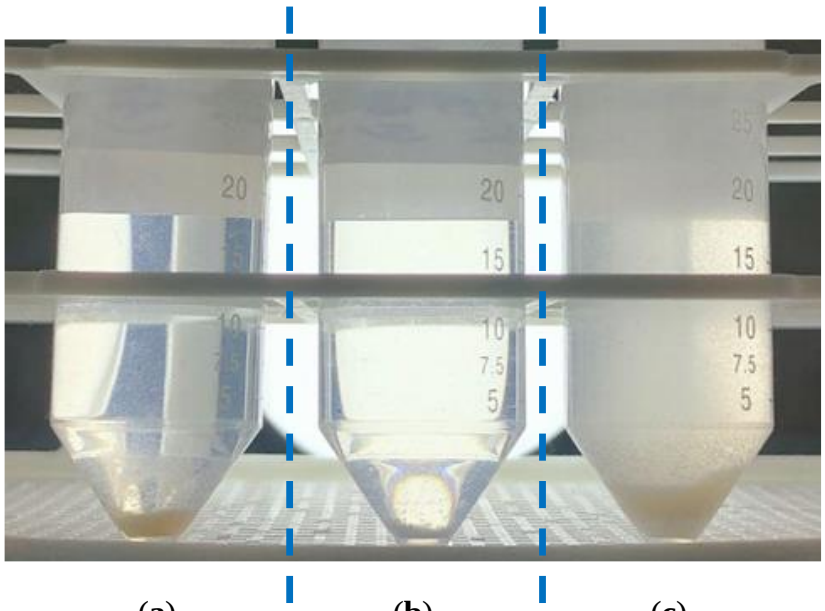


**Figure 6.** Photograph of 0.9 wt.% NaCl corrosion media with varying opacity and amount of corrosion sediment settled at the bottom of the test tube after 14 days of immersion for respective treatments; (**a**) without renewal of the corrosion media, MgNx, (**b**) with corrosion media renewal, MgNR, and (**c**) with Tris-HCl buffer reagent addition, MgNT.

As can be seen in Figure 5 (c), the trend of the corrosion rate in terms of mass loss is coherent with the corrosion rate calculated from the released $H_2$ volume, despite their noticeable value difference. Two contributing factors to these discrepancies are: (i) the overestimated corrosion rate in terms of mass loss is due to severe dislodge of the corrosion layer along with the metal substrate during chromic acid cleaning, which has resulted in excessive mass reduction [56], and (ii) the water displacement resulting from the released $H_2$ may be underestimated due to the challenging $H_2$ gas collecting procedure due to the trapped $H_2$ gas within the dome-like structure. The corrosion rate of CP Mg and Mg-1.0Ca-0.5Sr in 0.9 wt.% NaCl ranked in the following decreasing order: MgNT > MgNR > MgNx > M2NT > M2NR > M2Nx.

*3.4. Influence of 0.9 wt.% NaCl and pH regulation technique on the formation of corrosion protective layer.*

Any metal's magnitude of corrosion resistance lies on the nature or types of corrosion precipitation on its surface. The prediction of the corrosion precipitation variants and their order of formation during the immersion test was simulated via Hydra-Medusa software. The Hydra software selected all relevant ions within the corresponding corrosion media. Subsequently, the ionic concentrations of the respective corrosion media were set as the equilibrium concentration in the Medusa software, except for the $Mg^{2+}$, $Ca^{2+}$, and $Sr^{2+}$ concentrations. However, the $Mg^{2+}$, $Ca^{2+}$, and $Sr^{2+}$ concentration was calculated based on the final volume of the evolved $H_2$ before being added to their initial concentrations.

Figure 7 illustrates the Hydra-Medusa plot for CP Mg and Mg-1.0Ca-0.5Sr in 0.9 wt.% NaCl where the fraction of $Mg^{2+}$, $Ca^{2+}$ and $Sr^{2+}$ were plot against pH value. It is evident that the only precipitate formed in 0.9 wt.% NaCl is $Mg(OH)_2$, which was confirmed by the XRD analysis in Figure 8. Since $H_2$ evolution and $OH^-$ accumulation occur simultaneously, the lower cumulative $H_2$ volume released during the immersion test means that the $OH^-$ accumulation is also lower, indicating insufficient $OH^-$ ions and hence insufficient pH level to precipitate

$Mg(OH)_2$. Therefore, the lower $H_2$ release has to cause the pH to initiate the precipitation of $Mg(OH)_2$ to become higher and vice versa. For example, $Mg(OH)_2$ precipitation in M2Nx (cumulative $H_2$ released = 8.74 ml/cm$^2$) starts at pH 9.58, while brucite precipitation in MgNx (cumulative $H_2$ released = 38.18 ml/cm$^2$) starts at pH 9.23. This, in principle, yields the hypothesis that the immersed materials with high pH values signify better corrosion resistance. In addition, the simulated results agreed well with the experimental value in Figure 5 (b), where the prompt pH increase of M2Nx and MgNx starts to decrease at pH 9.55 and 9.22, respectively, indicating that the initiation of protective layer formation has been reached. These results justify that the rapid $H_2$ during the early immersion aims to reach the pH for the precipitation of the $Mg(OH)_2$ layer.

A negligible pH difference was observed to initiate the formation of $Mg(OH)_2$ in M2Nx and M2NR (at hour 24), indicating better degradation control attributed to the alloying technique. Meanwhile, due to the fast and unstable dissolution nature of CP MG, a noticeable difference was seen between MgNx and MgNR in the same time frame.

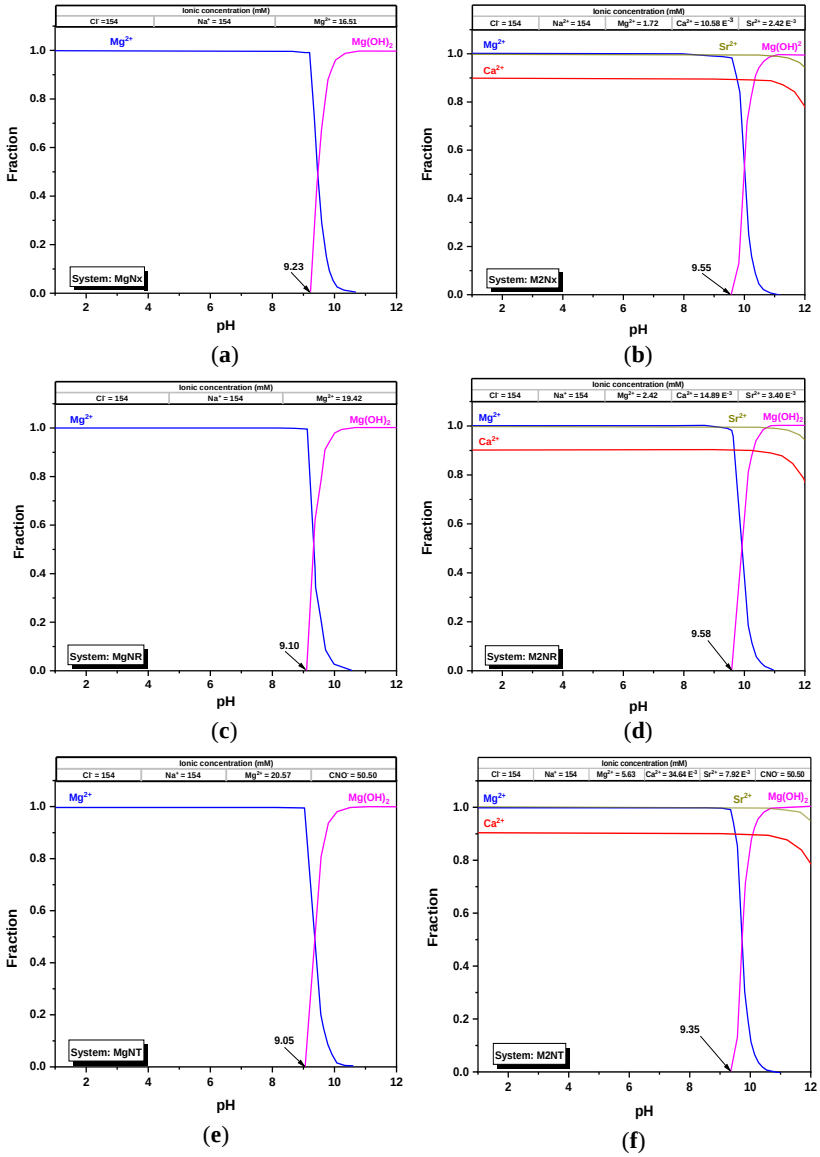


**Figure 7.** Simulated Hydra-Medusa diagram of either $Mg^{2+}$, $Ca^{2+}$, or $Sr^{2+}$ fraction against pH value based on thermodynamic constant. (**a**,**c,** and **e**) display the simulated diagram with the predicted precipitate of CP Mg in saline solution under three treatment conditions. (**b**, **d**, and **f**) illustrate the possible precipitate resulting from Mg-1.0Ca-0.5Sr alloy immersion. The labeled pH values indicate the minimum pH value to initiate the formation of $Mg(OH)_2$.

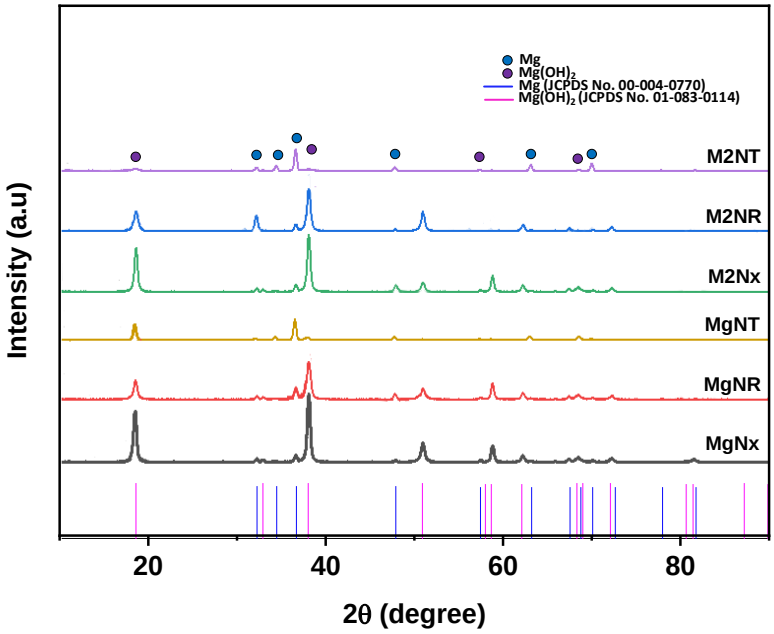


**Figure 8.** XRD peaks of Cp Mg and Mg-1.0Ca-0.5Sr alloy after 14 days immersion in 0.9 wt.% NaCl corrosion media under different pH control conditions.

However, the $Mg(OH)_2$ precipitation in MgNT and M2NT starts at pH 9.05 and 9.35, which were not reached during the experiment. These results explain that the Tris-HCL buffered systems have difficulty forming the protective layer, increasing the corrosion rate for both CP Mg and Mg-1.0Ca-0.5Sr alloy.

It also can be seen that the dissolution of $Ca^{2+}$ and Sr2+ from Mg-1.0Ca-0.5Sr alloy into the 0.9 wt.% NaCl corrosion media does not combine with $OH^-$ ions to form any precipitates, which suggests that the improved corrosion resistance provided by the alloying elements was attributed to the grain refinement effect and the formation of an intermetallic phase that acts as the sacrificial anode to α-Mg matrix.

*3.5. Corrosion mechanism of CP Mg and Mg-1.0Ca-0.5Sr alloy in 0.9 wt.% NaCl.*

The immersion test in 0.9 wt.% NaCl showed a significant effect on alloying elements. Therefore, a schematic representation was illustrated for each material. In Figure 9 (a-b), the thin layer of MgO film formed in the atmosphere soon after polishing and immediately transformed into a thin layer of $Mg(OH)_2$ film upon contact with water. This thin primary layer of $Mg(OH)_2$ provides insufficient protection to CP Mg substrate due to its porous and thin properties. Thus, an active accumulation of $OH^-$ and $H_2$ released occurs simultaneously with the dissolution of the Mg substrate, increasing the local pH value, thereby allowing the formation of a thicker $Mg(OH)_2$ protection layer (Figure 9 (c)). However, the aggressive $Cl^-$ ions can still infiltrate this porous layer and degrade the underlying Mg substrate. The degree of corrosion became severe during the renewal of the corrosion media, where the solubility of $Mg(OH)_2$ in water became higher at a sudden pH drop (Figure 9 (d)). In addition, the reaction of the $Mg(OH)_2$ layer and $Cl^-$ ions produces the water-soluble $MgCl_2$, which further breaks the corrosion protection layer.

Interestingly, the rate of $Mg(OH)_2$ precipitation doubled during the second exposure of Mg to NaCl solution (Figure 9 (e)). This phenomenon has increased the corrosion layer thickness and made it difficult for NaCl or water to access the underlying Mg substrate, leading to dehydration of $Mg(OH)_2$ at the $Mg(OH)_2$/Mg interface. This dehydration transforms this

inner layer back to MgO, which serves as the second layer protection barrier. The formation of MgO spreads laterally and eventually covers the whole $Mg(OH)_2$/Mg interface (Figure 9 (f)), inhibiting the further dissolution of Mg substrate, thus the $H_2$ release and $OH^-$ accumulation. This is where a plateau stage in $H_2$ evolution or pH variation is normally observed. However, the MgO barrier will transform back to $Mg(OH)_2$ and be destroyed during the excessive partial dissolution of the front $Mg(OH)_2$, especially when involving corrosion media renewal.

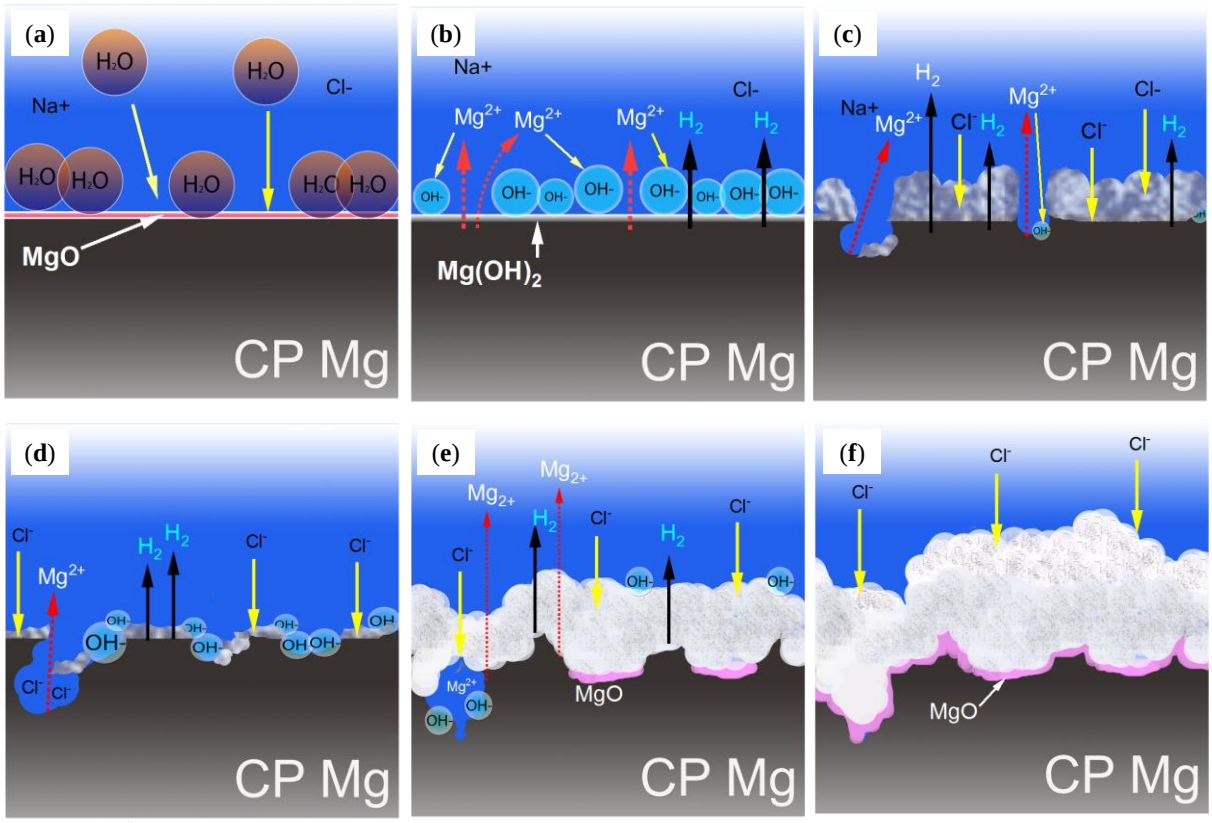


**Figure 9.** Schematic illustration of CP Mg corrosion mechanism in 0.9 wt.% NaCl corrosion media.

Meanwhile, Mg-1.0Ca-0.5Sr alloy exhibits a different corrosion mechanism due to its altered morphology through the alloying technique. The GBs in Figure 10 (a) showed two color gradients where the yellow area indicates the anodic $Mg_{17}Sr_2$ phase while the black area signifies the anodic $Mg_2Ca$ phase. At the initial immersion time, $Mg_2Ca$ preferentially corrodes due to its lower potential value compared to the adjacent α-Mg matrix. It gives off electrons to corrosion media and dissolves into $Mg^{2+}$ cations. The accumulation of $OH^-$ occurs at the cathodic α-Mg site, increasing the local pH and, thus, activating the formation of $Mg(OH)_2$ over its surface by the combination of the adsorbed $Mg^+$ and $OH^-$ ions. However, due to the anodic nature of $Mg_{17}Sr_2$ to the α-Mg, there is no dissolution of the corresponding GBs, but it micro-galvanically accelerates the corrosion of the adjacent α-Mg. In Figure 10 (b), the formation of $Mg(OH)_2$ is detrimentally attacked by the $Cl^-$ ions in the NaCl solution, which leads to a mass dissolution of α-Mg. Although the renewal routine further induces a severe corrosion reaction, the dissolution of α-Mg was stopped by the continuous network of $Mg_{17}Sr_2$, which is cathodically protected (Figure 10 (c-d)). A similar corrosion-inhibiting MgO transformation occurs after the accelerated and thickened $Mg(OH)_2$ precipitation.

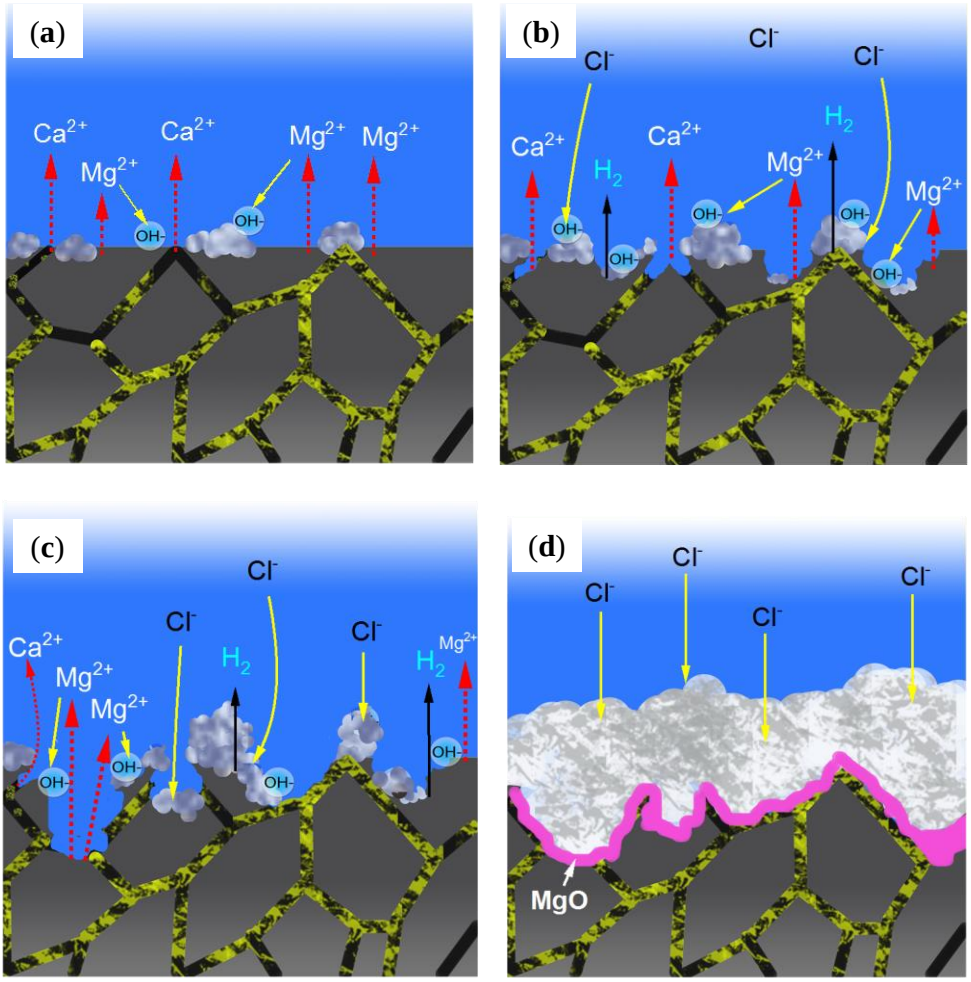


**Figure 10.** Corrosion mechanism of Mg-1.0Ca-0.5Sr alloy in 0.9 wt.% NaCl. The GBs was illustrated in two colors to imitate the lamellar structure in their GBs, with the yellow color indicating the $Mg_{17}Sr_2$ phase, while the black color suggests the distribution of $Mg_2Ca$ within the GBs.

## 4. Conclusions

The effects of pH regulating techniques on CP Mg and Mg-1.0Ca-0.5Sr alloy were investigated, and the following results were concluded:

The incorporation of Sr and Ca into the Mg-1.0Ca-0.5Sr alloy has shown a remarkable increase in corrosion resistance due to the compact and homogenous precipitation layer.

$Mg_2Ca$ acts as a sacrificial anode, protecting or retarding the dissolution of the α-Mg, while the $Mg_{17}Sr_2$ cathode accelerates the α-Mg dissolution in the early immersion stage, but inhibits intergranular corrosion propagation by forming a continuous barrier network in the GBs.

The $Mg(OH)_2$ layer is the only corrosion deposit formed on the Mg-1.0Ca-0.5Sr alloy, suggesting that the dissolution of $Mg_2Ca$ into $Ca^{2+}$ ions near the surface does not bind with the accumulated $OH^-$ ions. Therefore the alloying technique does not contribute to the increased corrosion resistance through the precipitation of novel anti-corrosion layers but through its grain-refining effect.

Despite the lack of inorganic and organic species with 0.9 wt.% NaCl solution, the utilization of the matched osmolality 0.9 wt.% NaCl is required when evaluating the intrinsic properties of the materials, such as the effects of alloying elements, surface treatments, and heat treatment, since the corrosion performance is not overestimated by the higher corrosion capacity of corrosion deposits precipitated by ionic species of the much complex corrosion

media. However, the utilization of more complex corrosion media reflects more on the *in vivo* response; thus, it is recommended to be utilized complementarily.

The utilization of Tris-HCl results in severe corrosion acceleration and should be avoided due to its incapability to regulate the pH near the material's surface, deviating from the goal of mimicking the human homeostasis response.

## Funding

This research was funded and supported by UTM Encouragement Research Grant no. Q.J130000.2651.17J44.

## Acknowledgments

The authors thank Wan Mohd Mazian in Metal Casting Laboratory for assisting with the synthesis and casting process and Nurul Husna Binti Jasin of the Faculty of Bioscience and Medical Engineering and the Centre for Composite (C*f*C) assistant engineers for making the biocorrosion facility and their expertise available to our work. The technical support of the Materials Engineering Laboratory's assistant engineers during the metallographic analysis is gratefully acknowledged.

## Conflicts of Interest

The authors declare no conflict of interest.

## References

1. Fernández, J.; El Ouardi, Y.; Bonastre, J.; Molina, J.; Cases, F., Modification of the magnesium corrosion rate in physiological saline 0.9 wt% NaCl via chemical and electrochemical coating of reduced graphene oxide. *Corrosion Science* **2019,** *152*, 75-81, https://doi.org/10.1016/J.CORSCI.2019.01.025.
2. Hanawa, T. In Recent development of new alloys for biomedical use, Materials science forum. *Trans Tech Publ:* **2006**; pp 243-248 https://doi.org/10.4028/www.scientific.net/MSF.512.243.
3. Xing, F.; Li, S.; Yin, D.; Xie, J.; Rommens, P. M.; Xiang, Z.; Liu, M.; Ritz, U., Recent progress in Mg-based alloys as a novel bioabsorbable biomaterials for orthopedic applications. *Journal of Magnesium and Alloys* **2022,** *10*, 1428-1456, https://doi.org/10.1016/j.jma.2022.02.013.
4. Godavitarne, C.; Robertson, A.; Peters, J.; Rogers, B., Biodegradable materials. *Orthopaedics and trauma* **2017,** *31*, 316-320, https://doi.org/10.1016/j.mporth.2017.07.011.
5. Tan, L.; Yu, X.; Wan, P.; Yang, K., Biodegradable materials for bone repairs: a review. *Journal of Materials Science & Technology* **2013,** *29*, 503-513, https://doi.org/10.1016/j.jmst.2013.03.002.
6. Chandra, G.; Pandey, A., Biodegradable bone implants in orthopedic applications: a review. *Biocybernetics and Biomedical Engineering* **2020,** *40*, 596-610, https://doi.org/10.1016/j.bbe.2020.02.003.
7. Driessen, M.; Goessens, M., Complications of implant removal after healed hip fractures. *Archives of Orthopaedic and Trauma Surgery* **2020,** *140*, 1745-1749, https://doi.org/10.1007/s00402-020-03435-1.
8. Mei, D.; Lamaka, S. V.; Gonzalez, J.; Feyerabend, F.; Willumeit-Römer, R.; Zheludkevich, M. L., The role of individual components of simulated body fluid on the corrosion behavior of commercially pure Mg. *Corrosion Science* **2019,** *147*, 81-93, https://doi.org/10.1016/j.corsci.2018.11.011.
9. Tsakiris, V.; Tardei, C.; Clicinschi, F. M., Biodegradable Mg alloys for orthopedic implants–A review. *Journal of Magnesium and Alloys* **2021,** *9*, 1884-1905, https://doi.org/10.1016/j.jma.2021.06.024.
10. Zhang, E. Phosphate treatment of magnesium alloy implants for biomedical applications. In *Surface modification of magnesium and its alloys for biomedical applications*, Elsevier: 2015; pp 23-57 https://doi.org/10.1016/B978-1-78242-078-1.00002-5.
11. Nasr Azadani, M.; Zahedi, A.; Bowoto, O. K.; Oladapo, B. I., A review of current challenges and prospects of magnesium and its alloy for bone implant applications. *Progress in Biomaterials* **2022,** *11*, 1-26, https://doi.org/10.1007/s40204-022-00182-x.
12. Kumar, R.; Katyal, P., Effects of alloying elements on performance of biodegradable magnesium alloy. *Materials Today: Proceedings* **2022,** *56*, 2443-2450, https://doi.org/10.1016/j.matpr.2021.08.233.
13. Li, H.; Lin, G.; Wang, P.; Huang, J.; Wen, C., Nutrient alloying elements in biodegradable metals: a review. *Journal of Materials Chemistry B* **2021,** *9*, 9806-9825, https://doi.org/10.1039/d1tb01962g.

14. Maji, K.; Mondal, S. Calcium phosphate biomaterials for bone tissue engineering: Properties and relevance in bone repair. In *Racing for the Surface*, Springer: **2020**, 535-555, https://doi.org/10.1007/978-3-030-34471-9_20.
15. Hebert, S. C., Extracellular calcium-sensing receptor: implications for calcium and magnesium handling in the kidney. *Kidney international* **1996,** *50*, 2129-2139, https://doi.org/10.1038/ki.1996.539.
16. Peacock, M., Calcium metabolism in health and disease. *Clinical Journal of the American society of nephrology* **2010,** *5*, S23-S30, https://doi.org/10.2215/Cjn.05910809.
17. Mushahary, D.; Sravanthi, R.; Li, Y.; Kumar, M. J.; Harishankar, N.; Hodgson, P. D.; Wen, C.; Pande, G., Zirconium, calcium, and strontium contents in magnesium based biodegradable alloys modulate the efficiency of implant-induced osseointegration. *International journal of nanomedicine* **2013,** *8*, 2887-2902, https://doi.org/10.2147/Ijn.S47378.
18. Lu, W.; Zhou, C.; Ma, Y.; Li, J.; Jiang, J.; Chen, Y.; Dong, L.; He, F., Improved osseointegration of strontium-modified titanium implants by regulating angiogenesis and macrophage polarization. *Biomaterials Science* **2022,** *10*, 2198-2214, https://doi.org/10.1039/d1bm01488a.
19. Mei, D.; Lamaka, S. V.; Lu, X.; Zheludkevich, M. L., Selecting medium for corrosion testing of bioabsorbable magnesium and other metals–a critical review. *Corrosion Science* **2020,** *171*, 108722, https://doi.org/10.1016/j.corsci.2020.108722.
20. Zhao, M.-C.; Liu, M.; Song, G.-L.; Atrens, A., Influence of pH and chloride ion concentration on the corrosion of Mg alloy ZE41. *Corrosion Science* **2008,** *50*, 3168-3178, https://doi.org/10.1016/j.corsci.2008.08.023.
21. Ng, W.; Chiu, K.; Cheng, F. Effect of pH on the *in vitro* corrosion rate of magnesium degradable implant material. *Materials Science and Engineering: C* **2010,** *30*, 898-903, https://doi.org/10.1016/j.msec.2010.04.003.
22. Xin, Y.; Chu, P. K. Influence of Tris in simulated body fluid on degradation behavior of pure magnesium. *Materials Chemistry and Physics* **2010,** *124*, 33-35, https://doi.org/10.1016/j.matchemphys.2010.07.010.
23. He, L.; Yang, J.; Xiong, Y.; Song, R., Effect of solution pH on stress corrosion cracking behavior of modified AZ80 magnesium alloy in simulated body fluid. *Materials Chemistry and Physics* **2021,** *261*, 124232, https://doi.org/10.1016/j.matchemphys.2021.124232.
24. Liu, X.; Yang, H.; Xiong, P.; Li, W.; Huang, H.-H.; Zheng, Y., Comparative studies of Tris-HCl, HEPES and $NaHCO_3/CO_2$ buffer systems on the biodegradation behaviour of pure Zn in NaCl and SBF solutions. *Corrosion Science* **2019,** *157*, 205-219, https://doi.org/10.1016/j.corsci.2019.05.018.
25. Batool, Z.; Wang, M.; Chen, J.; Ma, M.; Chen, F., Regulation of physiological pH and consumption of potential food ingredients for maintaining homeostasis and metabolic function: An overview. *Food Reviews International* **2022,** 1-17, https://doi.org/10.1080/87559129.2022.2062379.
26. Amukarimi, S.; Mozafari, M., Biodegradable Magnesium Biomaterials—Road to the Clinic. *Bioengineering* **2022,** *9*, 107, https://doi.org/10.3390/bioengineering9030107.
27. Mei, D.; Lamaka, S. V.; Feiler, C.; Zheludkevich, M. L., The effect of small-molecule bio-relevant organic components at low concentration on the corrosion of commercially pure Mg and Mg-0.8 Ca alloy: an overall perspective. *Corrosion Science* **2019,** *153*, 258-271, https://doi.org/10.1016/j.corsci.2019.03.039.
28. Stone-Weiss, N.; Smith, N. J.; Youngman, R. E.; Pierce, E. M.; Goel, A., Dissolution kinetics of a sodium borosilicate glass in Tris buffer solutions: impact of Tris concentration and acid (HCl/HNO 3) identity. *Physical Chemistry Chemical Physics* **2021,** *23*, 16165-16179, https://doi.org/10.1039/D0CP06425D.
29. Shi, Z.; Atrens, A., An innovative specimen configuration for the study of Mg corrosion. *Corrosion Science* **2011,** *53*, 226-246, https://doi.org/10.1016/j.corsci.2010.09.016.
30. Bornapour, M.; Celikin, M.; Pekguleryuz, M., Thermal exposure effects on the *in vitro* degradation and mechanical properties of Mg–Sr and Mg–Ca–Sr biodegradable implant alloys and the role of the microstructure. *Materials Science and Engineering: C* **2015,** *46*, 16-24, https://doi.org/10.1016/j.msec.2014.10.008.
31. Berglund, I. S.; Brar, H. S.; Dolgova, N.; Acharya, A. P.; Keselowsky, B. G.; Sarntinoranont, M.; Manuel, M. V., Synthesis and characterization of Mg-Ca-Sr alloys for biodegradable orthopedic implant applications. *Journal of Biomedical Materials Research Part B: Applied Biomaterials* **2012,** *100*, 1524-1534, https://doi.org/10.1002/jbm.b.32721.
32. Yu, H.-s.; Guo, X.-f.; Cui, H.-b. Microstructures and tensile properties of as-cast Mg-5Sn-1Si magnesium alloy modified with trace elements of Y, Bi, Sb and Sr. *China Foundry* **2021,** *18*, 9-17, https://doi.org/10.1007/s41230-021-0117-8.
33. Malekan, M.; Bahmani, A. Determination of dendrite coherency point characteristics in Al-Si-Mg alloy. *International Journal of Cast Metals Research* **2021,** *34*, 14-20, https://doi.org/10.1080/13640461.2020.1864928.
34. Zeng, R.-C.; Qi, W.-C.; Cui, H.-Z.; Zhang, F.; Li, S.-Q.; Han, E.-H., *In vitro* corrosion of as-extruded Mg–Ca alloys—the influence of Ca concentration. *Corrosion Science* **2015,** *96*, 23-31, https://doi.org/10.1016/j.corsci.2015.03.018
35. Seong, J.; Kim, W., Mg-Ca binary alloy sheets with Ca contents of≤ 1 wt.% with high corrosion resistance and high toughness. *Corrosion Science* **2015,** *98*, 372-381, https://doi.org/10.1016/j.corsci.2015.05.068.

36. Harandi, S. E.; Mirshahi, M.; Koleini, S.; Idris, M. H.; Jafari, H.; Kadir, M. R. A., Effect of calcium content on the microstructure, hardness and in-vitro corrosion behavior of biodegradable Mg-Ca binary alloy. *Materials Research* **2013,** *16*, 11-18, https://doi.org/10.1590/S1516-14392012005000151.
37. Jeong, Y.; Kim, W., Enhancement of mechanical properties and corrosion resistance of Mg–Ca alloys through microstructural refinement by indirect extrusion. *Corrosion Science* **2014,** *82*, 392-403, https://doi.org/10.1016/j.corsci.2014.01.041.
38. StJohn, D. H.; Qian, M.; Easton, M. A.; Cao, P.; Hildebrand, Z., Grain refinement of magnesium alloys. *Metallurgical and Materials Transactions A* **2005,** *36*, 1669-1679, https://doi.org/10.1007/s11661-005-0030-6.
39. Lee, Y.; Dahle, A.; StJohn, D., The role of solute in grain refinement of magnesium. *Metallurgical and Materials Transactions A* **2000,** *31*, 2895-2906, https://doi.org/10.1007/Bf02830349.
40. Johnston, S.; Dargusch, M.; Atrens, A., Building towards a standardised approach to biocorrosion studies: a review of factors influencing Mg corrosion *in vitro* pertinent to *in vivo* corrosion. *Science China Materials* **2018,** *61*, 475-500, https://doi.org/10.1007/s40843-017-9173-7.
41. Ma, W.; Liu, Y.; Wang, W.; Zhang, Y. Effects of electrolyte component in simulated body fluid on the corrosion behavior and mechanical integrity of magnesium. *Corrosion Science* **2015,** *98*, 201-210, https://doi.org/10.1016/j.corsci.2015.05.012.
42. Song, G.; Atrens, A. Understanding magnesium corrosion—a framework for improved alloy performance. *Advanced engineering materials* **2003,** *5*, 837-858, https://doi.org/10.1002/adem.200310405.
43. Allavikutty, R.; Gupta, P.; Santra, T. S.; Rengaswamy, J., Additive manufacturing of Mg alloys for biomedical applications: Current status and challenges. *Current Opinion in Biomedical Engineering* **2021,** *18*, 100276, https://doi.org/10.1016/j.cobme.2021.100276.
44. Atrens, A.; Shi, Z.; Mehreen, S. U.; Johnston, S.; Song, G.-L.; Chen, X.; Pan, F., Review of Mg alloy corrosion rates. *Journal of Magnesium and Alloys* **2020,** *8*, 989-998, https://doi.org/10.1016/j.jma.2020.08.002.
45. Atrens, A.; Johnston, S.; Shi, Z.; Dargusch, M. S., Understanding Mg corrosion in the body for biodegradable medical implants. *Scripta Materialia* **2018,** *154*, 92-100, https://doi.org/10.1016/j.scriptamat.2018.05.021.
46. Thekkepat, K.; Han, H.-S.; Choi, J.-W.; Lee, S.-C.; Yoon, E. S.; Li, G.; Seok, H.-K.; Kim, Y.-C.; Kim, J.-H.; Cha, P.-R., Computational design of Mg alloys with minimal galvanic corrosion. *Journal of Magnesium and Alloys* **2022,** *10*, 1972-1980, https://doi.org/10.1016/j.jma.2021.06.019.
47. Ding, Y.; Li, Y.; Wen, C., Effects of $Mg_{17}Sr_2$ phase on the bio-corrosion behavior of Mg–Zr–Sr alloys. *Advanced Engineering Materials* **2016,** *18*, 259-268, https://doi.org/10.1002/adem.201500222.
48. Mohamed, A.; El-Aziz, A. M.; Breitinger, H.-G. Study of the degradation behavior and the biocompatibility of Mg–0.8 Ca alloy for orthopedic implant applications. *Journal of Magnesium and Alloys* **2019,** *7*, 249-257, https://doi.org/10.1016/j.jma.2019.02.007.
49. Wang, Y.; Wang, H.; Luo, X.; Ren, G.; Cheng, W.; Hou, H., The Effects of Second Phase on Microstructure and Properties of Degradable as-cast Mg-Zn-Ca Alloy for Intrauterine Device (IUD) Applications. *Int. J. Electrochem. Sci* **2022,** *17*, 2, https://doi.org/10.20964/2022.08.39.
50. Wu, J.; Cao, X.; Xu, C.; Dong, Y.; Di, X.; Zhang, J., Effect of Sr on the microstructure and corrosion properties of the as-cast Mg–Zn–Zr alloy. *International Journal of Materials Research* **2022,** *113*, 194-204, https://doi.org/10.1515/ijmr-2021-8264.
51. Wang, C.; Liu, X.; Mei, D.; Deng, M.; Zheng, Y.; Zheludkevich, M. L.; Lamaka, S. V., Local pH and oxygen concentration at the interface of Zn alloys in Tris-HCl or HEPES buffered Hanks' balanced salt solution. *Corrosion Science* **2022,** *197*, 110061, https://doi.org/10.1016/j.corsci.2021.110061.
52. Wang, L.; Shinohara, T.; Zhang, B.-P., XPS study of the surface chemistry on AZ31 and AZ91 magnesium alloys in dilute NaCl solution. *Applied Surface Science* **2010,** *256*, 5807-5812, https://doi.org/10.1016/j.apsusc.2010.02.058.
53. Nam, T. H.; Kim, S. H.; Kim, J. G.; Kim, S. K., Corrosion resistance of extruded Mg–3Al–1Zn alloy manufactured by adding CaO for the replacement of the protective gases. *Materials and Corrosion* **2014,** *65*, 577-581, https://doi.org/10.1002/maco.201206849.
54. Rad, H. R. B.; Idris, M. H.; Kadir, M. R. A.; Farahany, S., Microstructure analysis and corrosion behavior of biodegradable Mg–Ca implant alloys. *Materials & Design* **2012,** *33*, 88-97, https://doi.org/10.1016/j.matdes.2011.06.057.
55. Amukarimi, S.; Mozafari, M., Biodegradable magnesium-based biomaterials: An overview of challenges and opportunities. *MedComm* **2021,** *2*, 123-144, https://doi.org/10.1002/mco2.59.
56. Bornapour, M.; Mahjoubi, H.; Vali, H.; Shum-Tim, D.; Cerruti, M.; Pekguleryuz, M., Surface characterization, *in vitro* and *in vivo* biocompatibility of Mg-0.3 Sr-0.3 Ca for temporary cardiovascular implant. *Materials Science and Engineering: C* **2016,** *67*, 72-84, https://doi.org/10.1016/j.msec.2016.04.108.
57. Ott, N.; Schmutz, P.; Ludwig, C.; Ulrich, A., Local, element-specific and time-resolved dissolution processes on a Mg–Y–RE alloy–Influence of inorganic species and buffering systems. *Corrosion science* **2013,** *75*, 201-211, https://doi.org/10.1016/j.corsci.2013.06.003.

58. Ferreira, C. M.; Pinto, I. S.; Soares, E. V.; Soares, H. M., (Un) suitability of the use of pH buffers in biological, biochemical and environmental studies and their interaction with metal ions–a review. *Rsc Advances* **2015,** *5*, 30989-31003, https://doi.org/10.1039/c4ra15453c.
59. Ascencio, M.; Pekguleryuz, M.; Omanovic, S., An investigation of the corrosion mechanisms of WE43 Mg alloy in a modified simulated body fluid solution: the effect of electrolyte renewal. *Corrosion Science* **2015,** *91*, 297-310, https://doi.org/10.1016/j.corsci.2014.11.034.
60. Zeng, R.-C.; Hu, Y.; Guan, S.-K.; Cui, H.-Z.; Han, E.-H., Corrosion of magnesium alloy AZ31: The influence of bicarbonate, sulphate, hydrogen phosphate and dihydrogen phosphate ions in saline solution. *Corrosion Science* **2014,** *86*, 171-182, https://doi.org/10.1016/j.corsci.2014.05.006.
61. Brady, M.; Rother, G.; Anovitz, L.; Littrell, K.; Unocic, K.; Elsentriecy, H.; Song, G.-L.; Thomson, J.; Gallego, N.; Davis, B., Film breakdown and nano-porous Mg (OH) 2 formation from corrosion of magnesium alloys in salt solutions. *Journal of the Electrochemical Society* **2015,** *162*, C140, https://doi.org/10.1149/2.0171504jes.
62. Maltseva, A.; Shkirskiy, V.; Lefèvre, G.; Volovitch, P., Effect of pH on Mg (OH) 2 film evolution on corroding Mg by *in situ* kinetic Raman mapping (KRM). *Corrosion Science* **2019,** *153*, 272-282, https://doi.org/10.1016/j.corsci.2019.03.024.
63. Straumanis, M.; Bhatia, B., Disintegration of magnesium while dissolving anodically in neutral and acidic solutions. *Journal of the Electrochemical Society* **1963,** *110*, 357, https://doi.org/10.1149/1.2425763.
64. Bairagi, D.; Mandal, S., A comprehensive review on biocompatible Mg-based alloys as temporary orthopaedic implants: Current status, challenges, and future prospects. *Journal of Magnesium and Alloys* **2021,** *10*, 627-669 https://doi.org/10.1016/j.jma.2021.09.005.
65. Xi, Y.; Xie, Z. Corrosion effects of magnesium chloride and sodium chloride on automobile components; Colorado Department of Transportation, Research [Branch]: **2002**, https://www.codot.gov/programs/research/pdfs/2002/magautocor.pdf.